ACS APPLIED MATERIALS & INTERFACES
Research Article
www.acsami.org

Thermal Stability of Organic Monolayers Grafted to Si(111): Insights from ReaxFF Reactive Molecular Dynamics Simulations

Federico A. Soria,[†,‡] Weiwei Zhang,[§] Adri C. T. van Duin,[§] and Eduardo M. Patrito*[,†]

[†]Departamento de Fisicoquímica and [‡]Departamento de Química Teórica y Computacional, Instituto de Investigaciones en Físico Química de Córdoba (INFIQC), Facultad de Ciencias Químicas, Universidad Nacional de Córdoba, X5000HUA Córdoba, Argentina

[§]Department of Mechanical and Nuclear Engineering, Pennsylvania State University, University Park, Pennsylvania 16802, United States

Supporting Information

ABSTRACT: We used the ReaxFF reactive molecular dynamics simulations to investigate the chemical mechanisms and kinetics of thermal decomposition processes of silicon surfaces grafted with different organic molecules via Si−C bonds at atomistic level. In this work, we considered the Si(111) surface grafted with n-alkyl (ethyl, propyl, pentyl, and decyl) layers in 50% coverage and, Si−CH_3, Si−$CCCH_3$ and Si−$CHCHCH_3$ layers in full coverage. Si radicals primarily formed by the homolytic cleavage of Si−C bonds play a key role in the dehydrogenation processes that lead to the decomposition of the monolayers. Contrary to commonly proposed mechanisms that only involve a single Si atom center, we found that the main decomposition pathways require two Si lattice atoms to proceed. The ability of surface silyl radicals to dehydrogenate the organic molecules depends on the flexibility of the carbon backbones of the organic molecules as well as on the C−H bond strength. The dehydrogenation of n-alkyl chains mainly involves the H atoms of the β-carbon (leading to 1-alkene desorption). However, as the surface coverage decreases, the flexibility of the alkyl chains allows for the dehydrogenation of any methylene group and even the terminal methyl group of the long decyl layer. On the contrary, the rigid carbon backbone of the Si−$CCCH_3$ and Si−$CHCHCH_3$ moieties hinders the dehydrogenation of the terminal methyl group, which confers these layers a higher thermal stability. For all layers, the surface ends up mostly hydrogenated as Si−C bonds break and new Si−H bonds are formed during the dehydrogenation reactions.

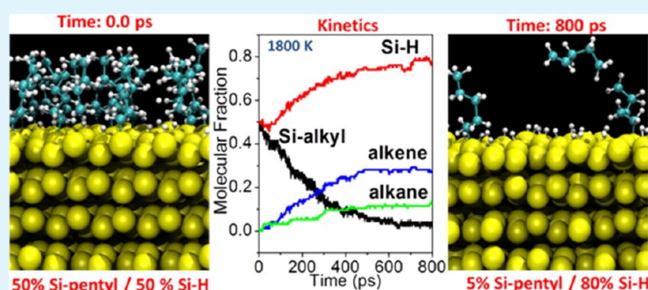

KEYWORDS: *silicon, functionalization, organic monolayer, thermal stability, molecular dynamics, ReaxFF*

INTRODUCTION

Silicon surface chemistry is of fundamental importance because of the ubiquitous role of silicon in modern technology. In a seminal paper, Linford and Chidsey showed that silicon−carbon bonds may be formed by the hydrosilylation of alkenes on hydrogen-terminated surfaces.[1] Since then, monolayer grafting has matured as a versatile method to tune the surface properties of semiconductor surfaces. The high reactivity of alkenes and alkynes toward silyl radicals has been employed as a major route for the formation of covalently bound organic monolayers on silicon.[2−5] The high stability of Si−C bonds and the versatile chemistry available for surface functionalization are the basis for the development of a large number of applications ranging from surface passivation[6−8] to silicon nanoparticle-based drug delivery,[9,10] molecular electronics,[11,12] photonics,[13−15] biosensing,[16,17] and photovoltaic devices.[18]

In microelectronics applications, the native silicon oxide has proven problematic as the sizes of silicon devices decrease[19] and there is a need of new chemical approaches toward the passivation of silicon surfaces in replacement of silicon dioxide. Passivation with organic monolayers has proved to be an efficient method to inhibit the growth of interfacial SiO_2 during the chemical vapor deposition of high-dielectric-constant oxides, such as HfO_2.[20,21] As these applications require processing at temperatures higher than ambient, the thermal stability of the organic layers thus becomes an important issue.

The thermal stability of alkyl-grafted silicon surfaces has been recently reviewed.[22] The nature of surface species has been identified using high-resolution electron energy loss spectroscopy (HREELS), synchrotron X-ray photoelectron spectroscopy (SXPS) (Si 2p and C 1s emissions), and in situ infrared (IR) spectroscopy (Si−H, C−H, and C−C stretching modes together with CH_2 rocking and CH_3 umbrella modes).[23] The comparison of results reported by different groups is not straightforward due to different heating protocols and possible oxygen contamination. HREELS,[23] IR,[24] and SXPS[25] studies have shown that as Si−C bonds break during the thermal desorption of alkyl layers, new Si−H bonds are formed. From these observations, it has been inferred that the desorption process occurs according to a β-elimination mechanism

Received: April 20, 2017
Accepted: August 16, 2017
Published: August 16, 2017

 © 2017 American Chemical Society

DOI: 10.1021/acsami.7b05444
ACS Appl. Mater. Interfaces 2017, 9, 30969−30981

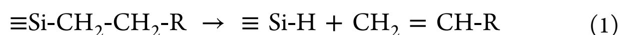

$$\equiv\text{Si-CH}_2\text{-CH}_2\text{-R} \rightarrow \equiv \text{Si-H} + \text{CH}_2 = \text{CH-R} \quad (1)$$

Equation 1 is reasonable as it is the reverse of the hydrosilylation reaction in the reaction of alkenes with the hydrogenated surface.[1−3]

An irreversible conformational disorder was observed for a C18 monolayer above 440 K;[26] however, the length of the alkyl chain was not found to affect the desorption temperature, except for the short C2 chain, which was reported to be more stable.[27] The appearance of a vibrational mode characteristic of the Si−CH_3 group has led to the conclusion that a secondary desorption mechanism could be operative at high temperatures for long alkyl chains according to

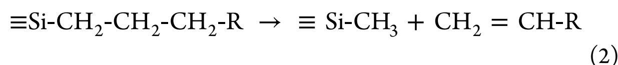

$$\equiv\text{Si-CH}_2\text{-CH}_2\text{-CH}_2\text{-R} \rightarrow \equiv \text{Si-CH}_3 + \text{CH}_2 = \text{CH-R} \quad (2)$$

as a consequence of the breakage of C−C bonds of the alkyl chain.[24,27] However, surface Si−CH_3 groups were also detected during the decomposition of a C2 layer, and it was proposed to proceed according to[25]

$$\equiv\text{Si-C}_2\text{H}_5 \rightarrow \equiv \text{Si-CH}_3 + \text{CH}_{2(\text{gas})} \quad (3)$$

Methylated surfaces have no SiH groups because the methyl group is atop all surface Si atoms with the covalent Si−C bond oriented normal to the surface.[28,29] Its thermal stability is higher than for longer alkyl chains,[25,28] and at high temperatures, the formation of silicon carbide was observed.[25,30] The superior stability of the methylated silicon surface has been attributed to the fact that the β-desorption mechanism (eq 1) is not operative for methyl. In the only investigation of desorption products reported, the CH_3^+ and $SiCH_3^+$ fragments were detected in time-of-flight mass spectrometry experiments.[31] Methyl groups were observed up to desorption temperatures of 1030 K, indicating the chemical robustness of the Si−CH_3 surface.

The Si(111) surface can also be fully covered with propynyl[32] (−$CCCH_3$) and 1-propenyl[33] (−$CHCHCH_3$) groups. The Si−$CCCH_3$ surface was reported to have a lower thermal stability than the Si−CH_3 surface. The reduction in the C 1s signal intensity observed in SXPS upon heating was interpreted as a reduction in the coverage of Si(111) surface sites by propynyl groups.[34] The Si−$CHCHCH_3$ surface was found to be more robust against surface oxidation and more stable against water attacks than the Si−$CCCH_3$ and Si−CH_3 surfaces.[33]

From a theoretical point of view, the functionalization of Si(111)-H has been investigated using density functional theory (DFT) calculations.[35−41] The radical chain reaction between silicon dangling bonds on the hydrogenated Si(111) surface and different alkenes was first investigated by Selloni and coworkers.[35,36] However, the thermal and chemical stabilities of Si(111) functionalized with Si−C bonds have been much less investigated. We have investigated the reactivity of Si(111)-H and different Si−C−R surfaces toward oxidizing agents, such as H_2O and O_2, at DFT level.[37−39] The diffusion of H_2O and O_2 through the compact Si−CH_3, Si−$CCCH_3$, and Si−$CHCHCH_3$ layers occurs with higher-energy barriers than through the Si−$CH_2CH_2CH_3$ layer[39] in agreement with the experimental observation that the former are more efficient for inhibiting the silicon oxidation.[8]

An important issue to understand the reactivity of surface silicon atoms with grafting molecules is the ability of silicon to form pentacoordinated complexes. This implies that surface silicon atoms (already back-bonded to three Si atoms in the second layer) can form two more bonds. As a consequence, silicon surface reactions have many intermediates giving rise to a rich chemistry.[40,41] For the Si (111) surface, this also implies that Si atoms in the second layer (coordinated to other four Si atoms) may also be involved in the surface chemistry, usually forming intermediates with diffusing molecules.[40,41]

Despite the importance of the surface chemistry of functionalized silicon, the underlying chemical mechanisms and kinetics of thermal decomposition of alkyl-grafted surfaces have not been studied yet in atomistic detail. In this work, we performed ReaxFF reactive molecular dynamics (MD) to identify the nature of adsorbed as well as gas-phase species during the thermal treatment of different alkyl layers on the Si(111) surface. ReaxFF enables the modeling of bond formation and breaking on the basis of a bond-order formalism.[42] Specifically, the goal of this work is to unveil the mechanisms of thermal decomposition, which may be helpful for a rational design of grafted surfaces with the best thermal stability. We considered two types of grafting molecules: (a) n-alkyl layers having a 50% of Si−C and 50% of Si−H coverage and (b) full-Si−C-coverage Si−CH_3, Si−$CCCH_3$, and Si−$CHCHCH_3$ layers. We show that silyl radicals play a key role in the dehydrogenation processes that lead to the decomposition of the monolayers. The flexible n-alkyl chains can be easily dehydrogenated at high temperatures, whereas the rigid backbone of the full-coverage propynyl and 1-propenyl monolayers imposes steric constraints that hinder H abstraction by adjacent silyl radicals.

■ MOLECULAR DYNAMICS MODELING

The ReaxFF force field provides an accurate description of bond breaking and bond formation during the MD simulations by employing a bond-order/bond-energy relationship, which was developed by van Duin, Goddard, and co-workers.[43,44] In this work, the Si/C/H force field parameters were optimized from a large training set of DFT calculations containing the main reactions involved in the decomposition of alkyl layers grafted onto Si(111). It thus describes very well pentacoordinated silicon, which is involved in many intermediates and transition states in the surface chemistry of silicon. The details of Si/C/H potential are described elsewhere.[45] A Velocity-Verlet algorithm was used with a 0.1 fs time step and a temperature-damping constant of 100 fs. The NVT/MD simulations were performed for 800 ps from 1500 to 2000 K. Prior to each simulation, the grafted silicon slab was thermalized at 300 K for 1 ps. All of the simulations were performed with the ADF2016[46] and LAMMPS[47] codes.

The Si(111) surface was represented by a slab with six silicon bilayers. In the external silicon bilayers, half of the atoms are on the surface plane. We will refer to them as the top atoms. They are coordinated to three atoms in the second layer (with three "backbonds") and expose a silyl radical. The atoms in the second layer are tetrahedrally coordinated to other Si atoms, but they are also involved in the surface bonding via the formation of pentacoordinated Si intermediates. We used 6×8 and $8\sqrt{3} \times 8$ unit cells with 48 and 64 silicon top atoms, respectively. The 6×8 cell was within a triclinic box with dimensions of 30.72 Å × 20.11 Å. The $8\sqrt{3} \times 8$ unit cell was within an orthogonal box of dimensions of 30.72 Å × 26.60 Å. The dimension along the z coordinate was 200 Å for both boxes.

DOI: 10.1021/acsami.7b05444
ACS Appl. Mater. Interfaces 2017, 9, 30969−30981

The alkylated surfaces were constructed with a 50% of hydrogenated Si top atoms and 50% of Si−alkyl groups. We considered ethyl (C2), propyl (C3), pentyl (C5), and decyl (C10) groups. SiH and Si−alkyl groups were randomly accommodated in either the 6 × 8 or $8\sqrt{3} \times 8$ unit cells. In the case of the $-CH_3$, $-CCCH_3$, and $-CHCHCH_3$ moieties, all Si top atoms were functionalized to obtain 100%-coverage monolayers. Silicon slabs were functionalized on both sides. The desorption mechanisms were independent of cell size or surface pattern produced by the random distribution of SiH and Si−alkyl groups. The smaller 6 × 8 cell was used for the long-term simulations (800 ps), whereas the larger $8\sqrt{3} \times 8$ cell was used to evaluate different surface patterns with short terms (200 ps). Figure S1 shows top and side views of the initial structures of all of the monolayers investigated.

As the decomposition of the organic monolayers involves the breaking of the strong Si−C, Si−H, and C−H bonds, high temperatures are required to allow chemical reactions to occur within a reasonable time scale in the MD simulations. It is known that the higher temperature is helpful to increase the decomposition reaction rate, but it might also lead to different reaction mechanisms. To make sure all of the reactions can be observed at more realistic temperatures, we first took the ethylated surface, which is the smallest model system, as an example to investigate the decomposition reactions in a wide temperature range of 1200−2200 K. We found that the same reaction processes were observed in this wide range but at very different time scales: nanosecond scale at temperatures lower than 1500 K, whereas picosecond scale at higher temperatures (>1500 K). At 1200 K, for example, the desorption of the first ethene molecule is observed after 3.5 ns, whereas several molecules desorb in less than 1 ns at the highest temperatures. The main reaction mechanism in the decomposition of the ethylated surface involves the desorption of ethene molecules, as shown in Figure S2, in the 1200−2200 K temperature range. Therefore, considering the computational cost, we simulated all of the other systems in the temperature range of 1500−2000 K, which can also capture the same chemical reactions as in a real experiment at lower temperatures. It should be mentioned that the melting point of silicon occurs at around 1600 K in experiment, which is lower than some of our simulation temperatures. However, we found that the silicon substrate remains crystalline in the present picosecond time scale. For example, the Si−Si pair correlation functions show the characteristic pattern for crystalline silicon, with the typical broadening of the peaks with increasing temperature (Figure S3). In addition, our previous studies showed that, on the picosecond scale, the temperature for silicon bulk melting with ReaxFF is up to around 3000 K (Figure S4); as such, on this time scale, the use of a temperature higher than the formal silicon melting temperature is justified.

RESULTS AND DISCUSSION

50%-Coverage n-Alkyl Monolayers. Figure 1 shows the variation of surface and gas-phase species during the decomposition of an ethylated surface at 1800 K. The decrease in the concentration of $Si-CH_2CH_3$ groups correlates with the increase of SiH groups. During the whole simulation, there is a small amount of silyl radicals that remains approximately constant (not shown here). Three species desorb to the gas phase: the ethyl radical and ethane and ethylene molecules. Figure 1 shows that the major gas-phase product is ethylene (26 molecules), followed by ethane (12 molecules). The Si−C

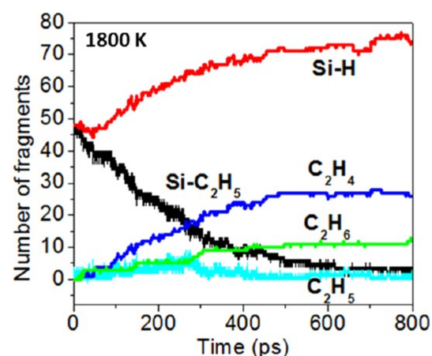

Figure 1. Variation in the amount of surface groups (SiH and $Si-C_2H_5$) and gas-phase products (C_2H_4, C_2H_6, and C_2H_5) for a silicon slab with a 50% coverage on both surfaces, having initially 48 SiH and 48 $Si-C_2H_5$ groups. Simulations were performed in a 6 × 8 unit cell at 1800 K.

bond cleavage leads to either the direct desorption of the ethyl radical or the formation of an ethane molecule by abstraction of a H atom from an adjacent SiH group. Figure 2 illustrates that the formation of an ethylene molecule occurs when an adjacent silyl radical abstracts a H atom from the methyl group of $Si-CH_2CH_3$. The snapshots in Figure 2 show a silyl radical close to $Si-CH_2CH_3$ group (Figure 2a), where the ethyl rotates so that the terminal methyl faces the silyl radical (Figure 2b). After the H abstraction (Figure 2c), ethylene is desorbed, leaving a SiH group and the newly formed silyl radical (Figure 2d). This mechanism can also be confirmed from Figure 1, where the formation of ethylene occurs after the ethyl and ethane desorption. This is because it requires the presence of silyl radicals, which are formed by the previous cleavage of Si−C bonds. In summary, the decomposition of the ethyl monolayer occurs as the following reaction pathways

$$\equiv \text{Si-CH}_2\text{CH}_3 \rightarrow \equiv \text{Si}^\bullet + {}^\bullet\text{CH}_2\text{CH}_{3(\text{gas})} \quad (4)$$

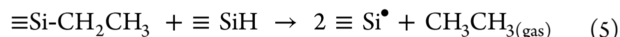

$$\equiv \text{Si-CH}_2\text{CH}_3 + \equiv \text{SiH} \rightarrow 2 \equiv \text{Si}^\bullet + \text{CH}_3\text{CH}_{3(\text{gas})} \quad (5)$$

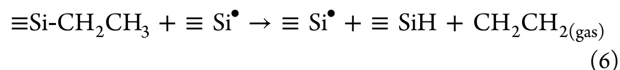

$$\equiv \text{Si-CH}_2\text{CH}_3 + \equiv \text{Si}^\bullet \rightarrow \equiv \text{Si}^\bullet + \equiv \text{SiH} + \text{CH}_2\text{CH}_{2(\text{gas})} \quad (6)$$

We remark that two silicon atoms are involved in reactions 5 and 6. Reactions 4 and 5 occur during the initial steps of the simulation (Figure 1), and they produce a small number of Si radicals, which remain approximately constant during the simulation. They are involved in the dehydrogenation of the ethyl species according to reaction 6. Then, the newly generated Si radical in reaction 6 dehydrogenates another ethyl species and thus reaction 6 occurs many times consuming the $Si-CH_2CH_3$ moieties, which finally produces a hydrogenated surface.

There are also other less likely reactions that were observed during the simulations. For example, when the ethyl radical is produced, it sometimes rotates above the $Si^\bullet$ radical, which thus may abstract a H atom from the methyl group, also leading to the formation of ethylene (Figure S5)

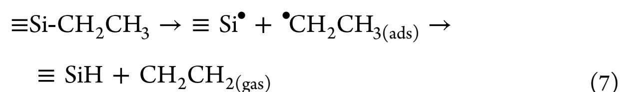

$$\equiv \text{Si-CH}_2\text{CH}_3 \rightarrow \equiv \text{Si}^\bullet + {}^\bullet\text{CH}_2\text{CH}_{3(\text{ads})} \rightarrow \equiv \text{SiH} + \text{CH}_2\text{CH}_{2(\text{gas})} \quad (7)$$

In the literature, it has been proposed[23−25] that desorption of alkyl chains as 1-alkenes involves only one Si atom as in eq 7

DOI: 10.1021/acsami.7b05444
ACS Appl. Mater. Interfaces 2017, 9, 30969−30981

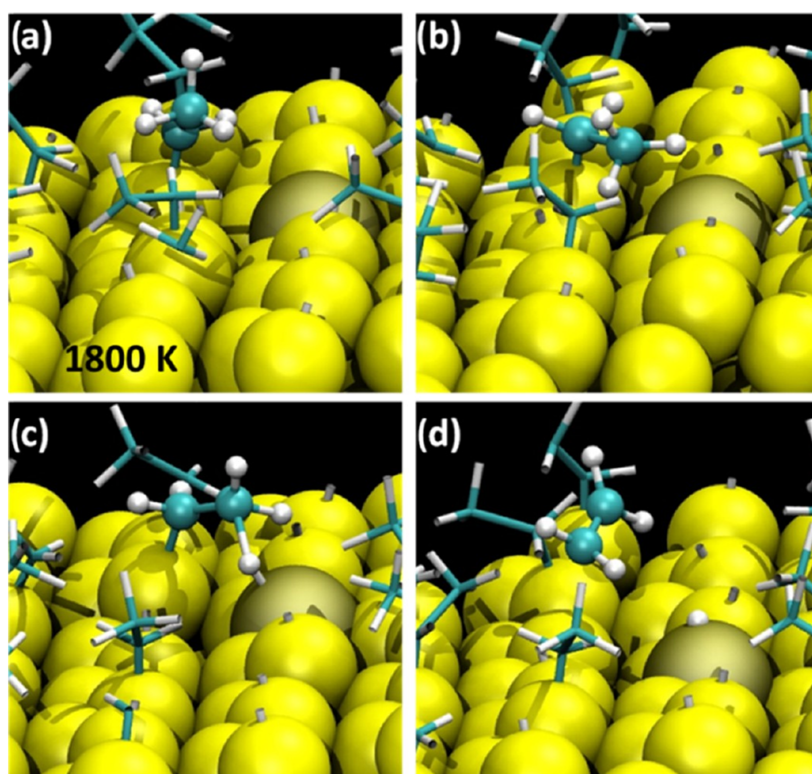

Figure 2. Snapshots during the reaction of an ethyl group with silyl radical (1800 K). (a) Ethyl group with an adjacent silyl radical formed by direct breakage of the Si−C bond; (b) terminal methyl group facing the silyl; (c) hydrogen abstraction; and (d) new SiH group formation and a CH_2CH_2 molecule leaving the surface.

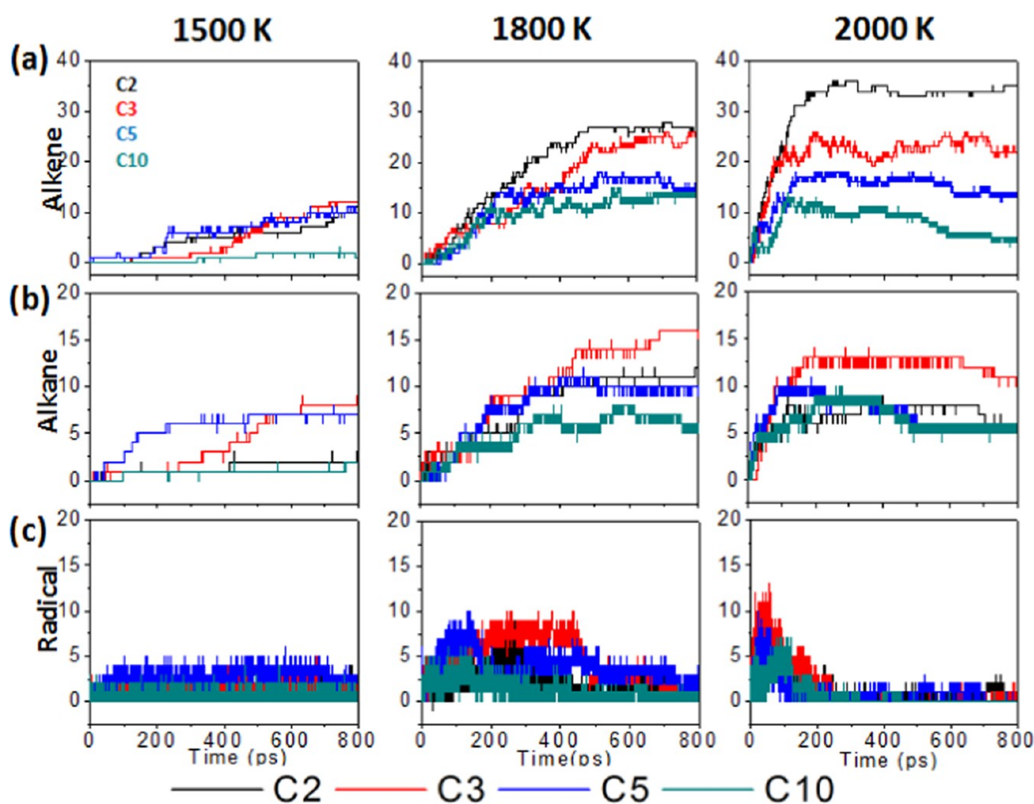

Figure 3. Number of molecules desorbed into the gas phase after the thermal treatment of C2, C3, C5, and C10 monolayers with a 50% surface coverage: (a) alkene, (b) alkane, and (c) alkyl radical species. Both sides of the silicon slab were functionalized. There are 48 SiH and 48 Si−alkyl groups in total initially. Simulations were performed in a 6 × 8 unit cell.

DOI: 10.1021/acsami.7b05444
ACS Appl. Mater. Interfaces 2017, 9, 30969−30981

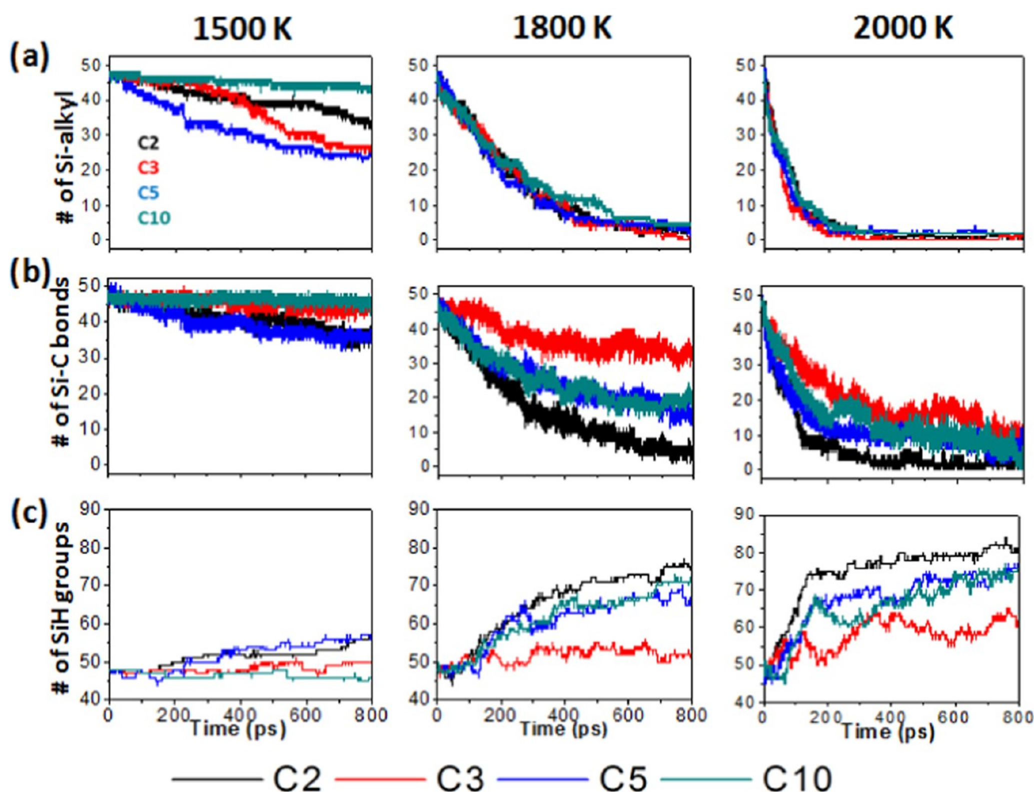

Figure 4. Number of surface species during the thermal treatment of C2, C3, C5, and C10 monolayers with an initial 50% surface coverage: (a) Si−alkyl groups (initially 48), (b) Si−C bonds, and (c) SiH groups. Simulations were performed with a 6 × 8 unit cell.

(or more generally as in eq 1). However, we remark that desorption of ethylene mainly occurred according to reaction 6, which involves two Si atoms. The analogue of reaction 7 for longer alkyl chains was never observed.

In addition, although the Si−C and Si−H bonds are strong bonds,[37] we observed that both the alkyl chains and H atoms diffuse during the course of the simulations. In the case of H atoms, this gives rise to the formation of dihydrides, which may eventually lead to desorption of H_2

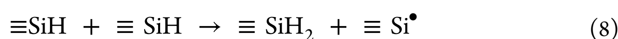

$$\equiv SiH + \equiv SiH \rightarrow \equiv SiH_2 + \equiv Si^{\bullet} \quad (8)$$

$$\equiv SiH_2 \rightarrow \equiv Si^{\bullet} + H_{2(gas)} \quad (9)$$

Equation 8 is a minority source of silyl radicals, whereas eq 9 is the main source of H_2. The formation of the SiH_2 species is an example of pentacoordination in the chemistry of silicon, as outlined in the Introduction section. Reaction 9 occurs within 3−5 ps, whereas the formation of the dihydride in eq 8 takes longer times (around 100 ps). This is consistent with the activation energy barriers of these reactions. Reaction 8 is the rate-limiting step with a barrier of 45.9 kcal/mol, whereas reaction 9 has a barrier of 23.4 kcal/mol (Figure S6). Our findings are consistent with the experimental observation that hydrogen desorption kinetics from H−Si(111) surfaces is second order in the high-coverage range.[48]

Figure 3 compares the three main gas-phase products (alkyl radical, alkane and alkene molecules) for different alkyl chain lengths and temperatures. In general, equivalent mechanisms are observed as for the Si−CH_2CH_3 layer case, as discussed above.

Irrespective of the alkyl chain length, the MD simulations showed that the 1-alkene molecule is the main desorption product, which is formed when an adjacent silyl radical abstracts a H atom from the *β*-carbon

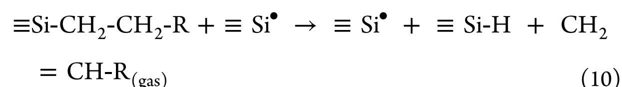

$$\equiv Si\text{-}CH_2\text{-}CH_2\text{-}R + \equiv Si^{\bullet} \rightarrow \equiv Si^{\bullet} + \equiv Si\text{-}H + CH_2 = CH\text{-}R_{(gas)} \quad (10)$$

The reaction mechanism of eq 10 is equivalent to that of eq 6 for ethyl-modified surface. An example of the formation of propene when a silyl radical abstracts a H atom from the *β*-carbon of a propyl group is shown in Figure S7. Therefore, the alkene formation involves two silicon atoms and not only one as proposed in the literature (see eq 1).[22−24] A reaction involving only one silicon atom would have a very low probability for long alkyl chains because after the breaking of the Si−C bond, the molecule is pushed away from the surface. As shown in eq 7, only for the ethyl monolayer we rarely observed the formation of an ethylene molecule involving only one Si atom.

In the case of the long C10 alkyl chain, desorption of decane molecules involves two steps

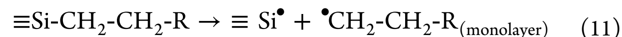

$$\equiv Si\text{-}CH_2\text{-}CH_2\text{-}R \rightarrow \equiv Si^{\bullet} + {}^{\bullet}CH_2\text{-}CH_2\text{-}R_{(monolayer)} \quad (11)$$

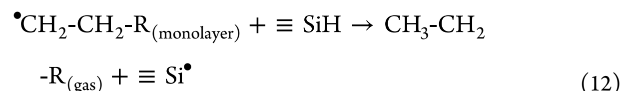

$${}^{\bullet}CH_2\text{-}CH_2\text{-}R_{(monolayer)} + \equiv SiH \rightarrow CH_3\text{-}CH_2\text{-}R_{(gas)} + \equiv Si^{\bullet} \quad (12)$$

After the cleavage of the Si−C bond, the radical stays within the monolayer (eq 11) and it may either recombine with the silyl radical (reverse of eq 11) or diffuse until it reacts with a SiH group to yield the alkane (eq 12). This is a clear example of the influence of the alkyl chain length on the desorption mechanism. The MD simulations showed that the interactions

DOI: 10.1021/acsami.7b05444
ACS Appl. Mater. Interfaces 2017, 9, 30969−30981

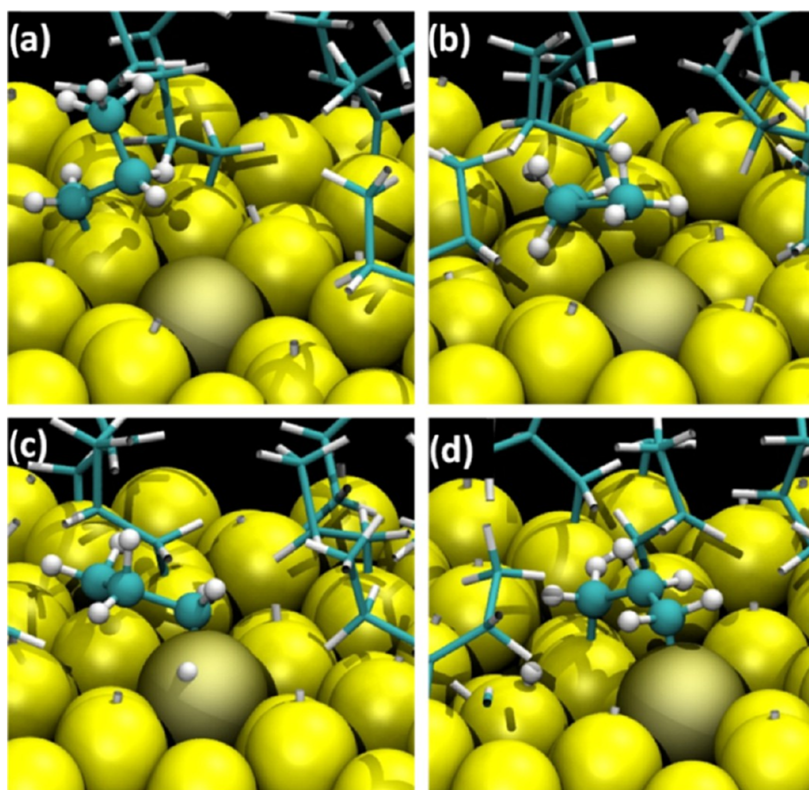

Figure 5. Snapshots showing the dehydrogenation of the terminal methyl group of Si-$CH_2CH_2CH_3$ (ball-and-stick model) by a silyl radical (dark yellow) to yield the bicoordinated Si−$CH_2CH_2CH_2$−Si species: (a) silyl radical adjacent to propyl group; (b) methyl group on top of silyl radical before the hydrogen abstraction; (c) formation of pentacoordinate Si atom with SiC and SiH bonds; and (d) hydrogen diffusion to adjacent silyl radical to yield SiH group.

among the long alkyl chains decrease the probability of Si−C bond breakage (eq 11) as well as the H abstraction from the β carbon (eq 10). In the latter case, a long alkyl chain imposes steric constraints that hinder favorable configurations for the H abstraction by an adjacent silyl radical. This explains the much lower 1-decene and decane desorption rates at 1500 and 1800 K (Figure 3) as compared to the shorter alkyl chains. However, at 2000 K, the initial desorption rate is independent of the alkyl chain length (the plots have approximately the same slope during the first 100 ps) indicating that the molecules have enough vibrational energy to overcome steric barriers.

Figure 4 shows the number of intact alkyl species bound to the surface (Si−alkyl), the number of SiH groups, and the number of Si−C bonds at different temperatures and for different alkyl chain lengths. Initially, the number of Si−alkyl groups (Figure 4a) and Si−C bonds (Figure 4b) is the same because every alkyl chain is bound to the surface by a Si−C bond. As the initial surface coverage is 50%, the number of Si−alkyl and SiH groups is also the same. However, as the dehydrogenation of the alkyl chains takes place, they may be coordinated to the surface by more than one Si−C bond. The decrease in the number Si−C bonds (Figure 4b) correlates with the increase in the number of SiH moieties (Figure 4c), which implies that the surface becomes progressively more hydrogenated as a consequence of Si−C bond cleavage. At the lowest temperature of 1500 K, the number of C10 molecules is higher than for the other chains (Figure 4a), whereas at the highest temperatures, a continued decrease in the number of alkyl chains is observed for all species.

Figure 4b shows that the number of Si−C bonds has an unexpected dependence with the chain length. The propyl layer, for example, has nearly the same number of Si−C bonds as the decyl layer at 1500 K, but at 1800 and 2000 K, it generates more Si−C bonds than the other layers. The fact that the C3 chains remain on the surface at the highest temperatures is due to the formation of bicoordinated Si−$CH_2CH_2CH_2$−Si moieties. We observed a competition between the dehydrogenation of the β-carbon (Figure S7) and the terminal −CH_3 group of propyl

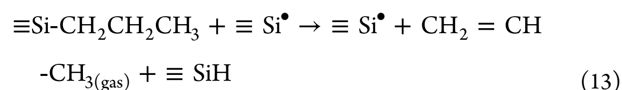

$$\equiv\text{Si-}CH_2CH_2CH_3 + \equiv \text{Si}^\bullet \rightarrow \equiv \text{Si}^\bullet + CH_2 = CH\text{-}CH_{3(gas)} + \equiv \text{SiH} \quad (13)$$

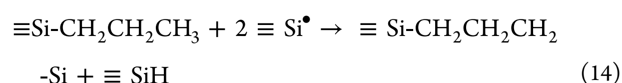

$$\equiv\text{Si-}CH_2CH_2CH_3 + 2 \equiv \text{Si}^\bullet \rightarrow \equiv \text{Si-}CH_2CH_2CH_2\text{-Si} + \equiv \text{SiH} \quad (14)$$

Equation 13 corresponds to the dehydrogenation of the β-carbon producing desorption of propene, whereas eq 14 refers to the formation of the bicoordinated moiety. Equation 14 is not an elementary reaction step, and the initial steps of this reaction are shown in Figure 5. The proximity of a silyl radical to a propyl group (Figure 5a) induces the rotation of the molecule so that the terminal methyl group approaches the silyl radical (Figure 5b). Then, the hydrogen abstraction occurs yielding the Si−$CH_2CH_2CH_2$−Si−H intermediate, where a Si atom is temporarily pentacoordinated (Figure 5c). Next, the H atom diffuses to an adjacent silyl radical (Figure 5d).

DOI: 10.1021/acsami.7b05444
ACS Appl. Mater. Interfaces 2017, 9, 30969−30981

A less likely observed reaction is the cleavage of the C−C bond and the transfer of the methyl group to an adjacent silyl radical (Figure S8)

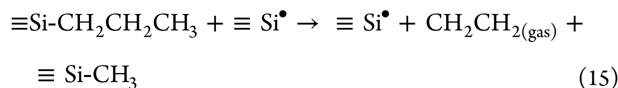

$$\equiv \text{Si-CH}_2\text{CH}_2\text{CH}_3 + \equiv \text{Si}^{\bullet} \rightarrow \equiv \text{Si}^{\bullet} + \text{CH}_2\text{CH}_{2(\text{gas})} + \equiv \text{Si-CH}_3 \quad (15)$$

Instead of abstracting a H atom from the terminal methyl group, the silyl radical promotes the cleavage of the C−C bond, giving rise to ethylene in the gas phase and the stable ≡Si−CH_3 moiety. The presence of small amounts of surface methyl groups has been reported experimentally during the decomposition of both long[24,27] and short alkyl chains,[25] and the proposed mechanisms involved one silicon atom, as given by eqs 2 and 3. However, we observed that an adjacent silyl radical is responsible for the breakage of the C−C bond according to eq 15. The mechanism in eq 15 may also be operative for long alkyl chains, as they have the flexibility to form lying-down and U-loop configurations, in which the terminal methyl group may approach silyl radical to yield Si−CH_3 moiety.

Figure 6 shows snapshots of the surface structure after thermal treatment at 1800 K for the C3, C5, and C10 layers with an initial surface coverage of 50% (32 Si−alkyl and 32 SiH groups for this unit cell). Figure 6a shows the surface structure of the propyl layer after 184 ps. There are nine bicoordinated molecules (ball-and-stick model), nine monocoordinated propyls (stick model), one Si−CH_3 species (red circle), and only four silyl radicals (dark yellow) out of a total of 64 Si surface atoms.

Figure 6b shows the surface structure of a pentyl layer after 228 ps at 1800 K. MD trajectories showed that silyl radicals may dehydrogenate any methylene group as well as the terminal −CH_3. The molecules represented with balls and sticks in Figure 6b are bicoordinated to the Si surface via Si−C bonds that involve different C atoms in the alkyl chain. The dehydrogenation of the fourth atom produces an unstable intermediate (Figure S9) whose methyl group releases a H atom to yield a stable terminal vinyl group (Figure S10)

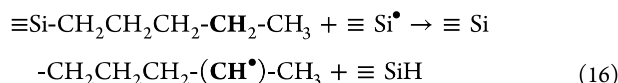

$$\equiv \text{Si-CH}_2\text{CH}_2\text{CH}_2\text{-}\mathbf{CH}_2\text{-CH}_3 + \equiv \text{Si}^{\bullet} \rightarrow \equiv \text{Si-CH}_2\text{CH}_2\text{CH}_2\text{-}(\mathbf{CH}^{\bullet})\text{-CH}_3 + \equiv \text{SiH} \quad (16)$$

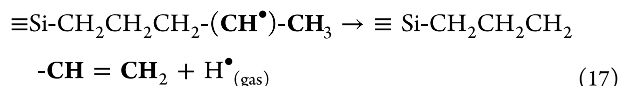

$$\equiv \text{Si-CH}_2\text{CH}_2\text{CH}_2\text{-}(\mathbf{CH}^{\bullet})\text{-}\mathbf{CH}_3 \rightarrow \equiv \text{Si-CH}_2\text{CH}_2\text{CH}_2\text{-}\mathbf{CH} = \mathbf{CH}_2 + \text{H}^{\bullet}_{(\text{gas})} \quad (17)$$

The red circles in Figure 6b,c show chains exposing a vinyl group. We remark that the presence of vinyl groups is an interesting feature, which appears for monolayers with four or more carbon atoms.

The snapshot of the C10 layer at 153 ps shows a lying-down species coordinated at both ends (Figure 6c). Even for this long-chain molecule, silyl radicals may abstract H atoms from the terminal methyl group as the molecule may either lay down or form a U-loop. Dehydrogenation of intermediate methylene groups leads to the breakage of C−C bonds. This is the reason for the appearance of a bicoordinated Si−CH_2CHCH_2−Si species (lower left in Figure 6c), an ethyl group (next to center), a hexyl species (upper right), and a bicoordinated Si−$CH_2CH(R)CH_2$−Si species (upper left) with R = $(CH_2)_5CH_3$. Dehydrogenation of the β-carbon by a silyl radical not only produces desorption of the alkene but sometimes induces the breakage of a C−C bond according to

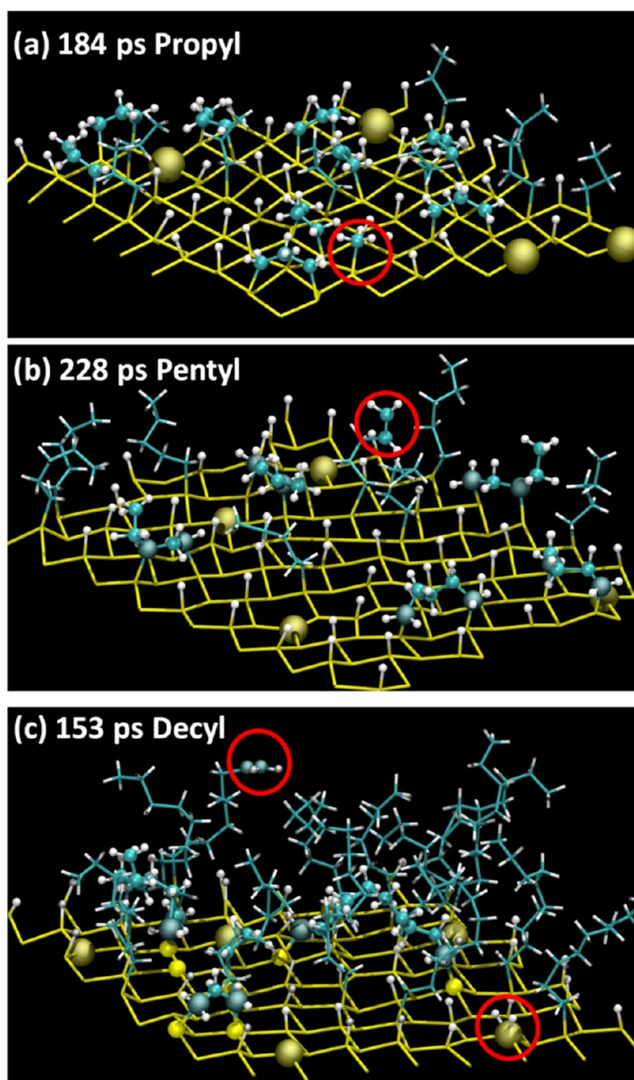

Figure 6. Surface composition at different simulation times for (a) propyl, (b) pentyl, and (c) decyl monolayers. Only the last Si bilayer is shown ($8\sqrt{3} \times 8$ unit cell with 64 silicon top atoms). Radical silicon atoms are shown in dark yellow. (a) Bicoordinated molecules are shown explicitly, whereas intact propyl groups are shown as a wireframe. The red circle shows a methyl group. (b) In bicoordinated pentyl molecules, the C atoms involved in Si−C bonds are marked in dark blue. Intact pentyl species are shown as a wireframe. The red circle shows a terminal vinyl group. (c) Bicoordinated molecules are shown explicitly, with the C atoms marked with dark blue. Intact decyl species are shown as a wireframe. The lower red circle shows a SiH_2 intermediate.

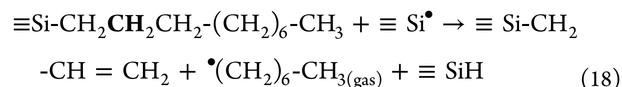

$$\equiv \text{Si-CH}_2\mathbf{CH}_2\text{CH}_2\text{-(CH}_2)_6\text{-CH}_3 + \equiv \text{Si}^{\bullet} \rightarrow \equiv \text{Si-CH}_2\text{-CH} = \text{CH}_2 + {}^{\bullet}(\text{CH}_2)_6\text{-CH}_{3(\text{gas})} + \equiv \text{SiH} \quad (18)$$

This reaction originated the Si−$CH_2CH{=}CH_2$ moiety shown in Figure 5c (which is temporarily bicoordinated due to the proximity to a silyl radical).

The fact that more bicoordinated structures are observed for the C3 layer than for the C5 and C10 layers is due to steric constraints. The MD simulations showed that the rotations of the propyl species around the Si−C and C−C bonds periodically located the terminal −CH_3 group very close to adjacent top Si atoms, which favors the hydrogen abstraction in the case of a silyl radical. For the longer alkyl chains, the

DOI: 10.1021/acsami.7b05444
ACS Appl. Mater. Interfaces 2017, 9, 30969−30981

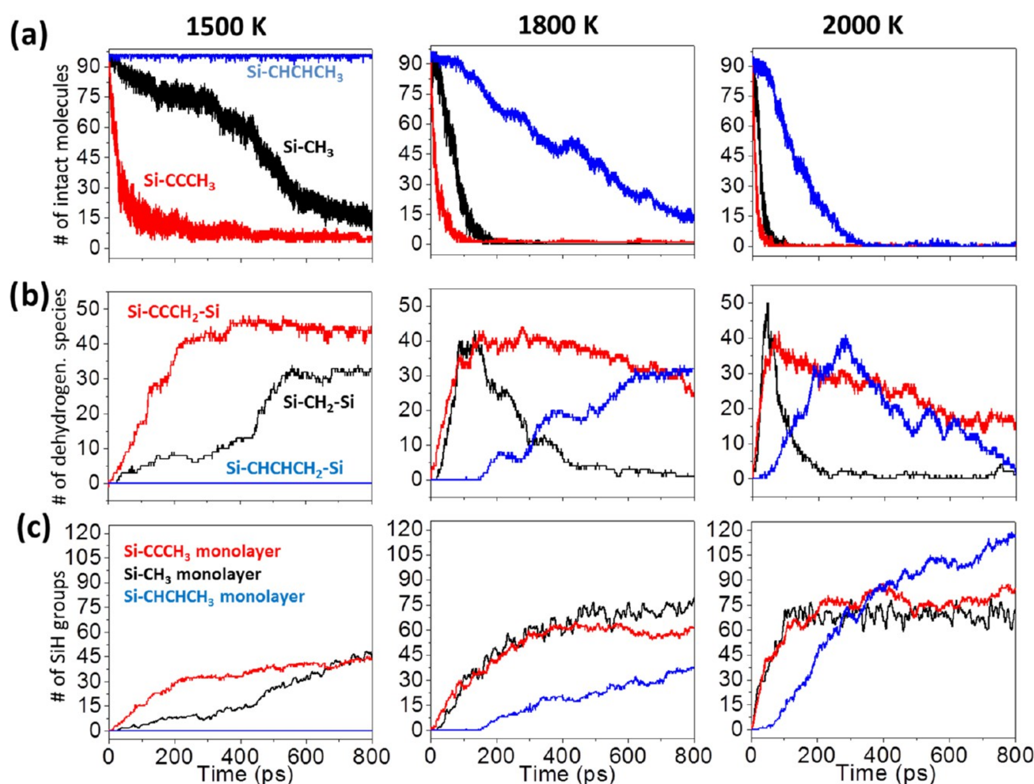

Figure 7. Comparison of the number of surface species for full-coverage Si−CH_3, Si−$CCCH_3$, and Si−$CHCHCH_3$ layers: (a) intact molecules; (b) dehydrogenated CH_2, $CCCH_2$, and $CHCHCH_2$ species; and (c) SiH groups appearing within the Si−CH_3, Si−$CCCH_3$, and Si−$CHCHCH_3$ layers. Simulations performed with a 6 × 8 unit cell with both sides of the silicon slab functionalized (96 molecules in total).

dehydrogenation of non-β C atoms occurs when the molecules are in lying-down or U-loop configurations, which is less likely.

In the case of a Si(111) surface grafted with a C18 monolayer, it was observed experimentally that the layer changed irreversibly after heating at high temperatures.[26] Under the light of our results, it becomes clear that the irreversible behavior originates from the partial dehydrogenation of the alkyl chains, which triggers the cleavage of C−C bonds, giving rise to shorter alkyl chains adsorbed on the surface, as shown in Figure 6c.

During the simulations, there is an approximately constant number of silyl radicals on the surface. Figure 6 shows that 4 top Si atoms are radicals (marked in dark yellow) from a total of 64 top Si atoms. In a previous work, we showed that these radicals are very reactive toward O_2 and H_2O, which leads the oxidation of the silicon backbonds.[38] This fact outlines the importance of avoiding oxygenated species in studies of the thermal stability of alkylated Si surfaces. In the case of a decyl monolayer, a limited oxidation of the Si surface was observed even under reducing atmosphere.[24] We suspect that many thermal studies may be affected by partial oxidation of Si, with the corresponding influence on the alkyl desorption kinetics.

Besides the desorption processes discussed so far, the diffusion of surface species also plays an important role in the monolayer dynamics. The mono- and bicoordinated alkyl chains as well as the H atoms of SiH groups diffuse until they react with silyl radicals. During this diffusion process, the alkyl chains may temporarily bind to hydrogenated Si atoms or to Si atoms in the second layer, producing pentacoordinated Si intermediates (R−CH_2−Si(Si)$_3$−H and R−CH_2−Si(Si)$_4$, respectively). The same holds for the diffusion of H atoms (yielding H_2Si(Si)$_3$ or H−Si(Si)$_4$ moieties). Figure S11 shows an example of the formation of pentacoordinated Si intermediates during the dehydrogenation of the terminal CH_3 group of a propyl molecule. During the formation of these intermediates, the silicon lattice dynamics plays an important role. The MD simulations show that Si atoms in the second layer (coordinated to other four Si atoms) eventually have strong upward displacements during the lattice vibrations, which makes them more reactive toward the formation of some of the pentacoordinated intermediates mentioned above. Similarly, the hydrogen abstraction by silyl radicals usually occurs after an upward displacement of the Si radical. This illustrates the ability of ReaxFF to handle the coupling of molecule−lattice vibrations, an effect with important consequences on the dynamics of chemical reactions on surfaces, which is very difficult to consider with ab initio methods.[49]

Full-Coverage Si−CH_3, Si−$CCCH_3$, and Si−$CHCHCH_3$ Monolayers. Figure 7 compares the amount of intact molecules bound to the Si surface (Si−CH_3, Si−$CCCH_3$, and Si−$CHCHCH_3$), dehydrogenated moieties, and surface SiH groups for the methyl-, propynyl-, and 1-propenyl-grafted silicon at three different temperatures. Figure 7a shows that the amount of intact molecules rapidly decreases, except for 1-propenyl. However, unlike the alkylated surfaces discussed above, it is found that the gas-phase desorption is considerably lower. The dehydrogenation processes produce the bicoordinated Si−CH_2−Si, Si−$CCCH_2$−Si, and Si−$CHCHCH_2$−Si surface species. Figure 7b shows that these moieties remain on the surface even at the highest temperature. The number of −CH_2− moieties shows a peak at 1800 and 2000 K and then it decreases to zero, which corresponds to further dehydrogenation processes accompanied by the formation of silicon carbide.

DOI: 10.1021/acsami.7b05444
ACS Appl. Mater. Interfaces 2017, 9, 30969−30981

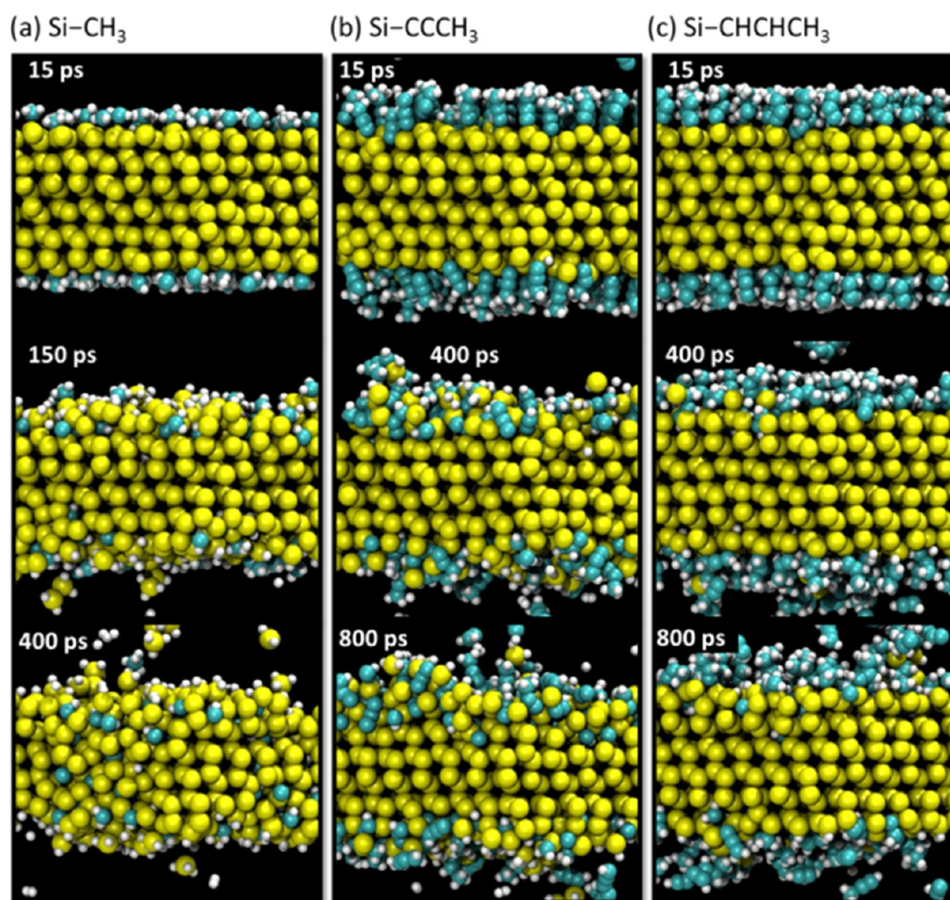

Figure 8. Side views of the silicon slab at different simulation times at 1800 K for the (a) Si−CH_3, (b) Si−$CCCH_3$, and (c) Si−$CHCHCH_3$ monolayers. Simulations were performed with a 6 × 8 unit cell.

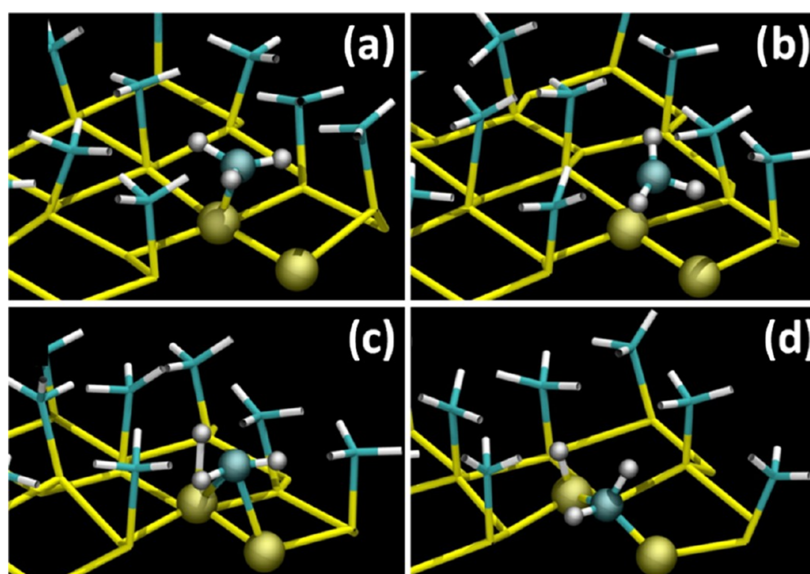

Figure 9. Most frequent dehydrogenation mechanism of the methyl group observed in the MD simulations. (a) A methyl group atop a Si atom (b) tilts toward a Si atom in the second layer until (c) a C−H bond is broken and a Si−H bond is formed. (d) Finally, the CH_2 group breaks the Si−Si backbond. All of these processes occur in 0.18 ps at 1500 K. Only part of the surface is shown for clarity.

Silyl radicals are involved in the dehydrogenation processes as for the alkylated surfaces, which originates an increase in the number of SiH groups (Figure 7c). Initially, there are no SiH groups as all of the Si top atoms are involved in Si−C bonds. At 1500 K, there are still no SiH groups for the Si−$CHCHCH_3$ monolayer because it does not decompose at this temperature. At 1800 K, SiH groups are generated by the dehydrogenation of the Si−$CHCHCH_3$ monolayer but the number is lower than

DOI: 10.1021/acsami.7b05444
ACS Appl. Mater. Interfaces 2017, 9, 30969−30981

for the other monolayers (Figure 7c). At 2000 K, a maximum of around 75 SiH groups are observed for the methyl and propynyl monolayers out of a total of 96 top Si atoms, indicating that most surface Si atoms are hydrogenated. The 1-propenyl monolayer produces more SiH groups than the number of top Si atoms because some H atoms diffuse into silicon.

Figure 8 shows snapshots at different simulation times at 1800 K comparing the stability of the Si−CH_3, Si−$CCCH_3$, and Si−$CHCHCH_3$ layers. At 15 ps, the monolayer structure is still preserved for all surfaces, except a just desorbed propynyl radical in the gas phase (Figure 8b). The decomposition of the methylated surface begins at 150 ps with an important dehydrogenation of CH_3 groups to yield CH_2 moieties, whereas the formation of SiC begins at 400 ps (Figure 8a). Overall, these processes are delayed in the time scale for the propynyl and 1-propenyl surfaces: the dehydrogenation of these monolayers begins at 400 ps, whereas a small amount of SiC begins to form at 800 ps for the propynyl surface (Figure 8b).

The snapshot at 400 ps for the methylated surface (Figure 8a) shows that the surface becomes nearly fully hydrogenated (as also shown in Figure 7c at 1800 K). The excess hydrogen is eliminated as H_2 and as different methyl silane species with formula $(CH_3)_xSiH_{4-x}$. Desorption of bare methyl radicals was not observed. Only a small fraction of the initial carbon content of the methylated surface is lost as methyl silanes and as methane. Our MD results for the methylated surface are in agreement with experimental results, which show the formation of silicon carbide at high temperatures[25,30] as well as desorption of silicon moieties.[31]

Figure 8b shows that some $CCCH_3$ and $HCCCH_3$ species eventually desorb. However, the number of such gas-phase species is much lower than that for the alkylated surfaces. The snapshot at 800 ps for the 1-propenyl surface (Figure 8c) shows that the monolayer structure is better preserved than for the propynyl surface. Very few CH_2CHCH_3 molecules desorb, whereas the surface species are a mixture of ≡Si−$CHCHCH_3$ and bicoordinated ≡Si−$CHCHCH_2$−Si≡ moieties.

Dehydrogenation Mechanisms of Full-Coverage Monolayers. The mechanism of dehydrogenation of the full-coverage monolayers remains still unclear in the literature. The MD simulations show that for the methylated surface, the most frequent dehydrogenation mechanism occurs when the methyl group jumps from the atop Si atom to an adjacent Si atom in the second layer, leaving behind a silyl radical. Figure 9 shows detailed snapshots of this process. The methyl group originally bound to the atop Si atom (Figure 9a) tilts toward an adjacent Si atom in the second layer (Figure 9b). This induces the simultaneous breakage of a C−H bond and the formation of a Si−H bond with the atop Si atom (Figure 9c). Finally, the CH_2 group cleaves the Si−Si backbond (Figure 9d). Globally, the reaction may be expressed as

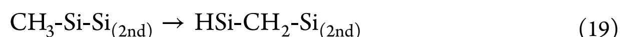

$$CH_3\text{-Si-Si}_{(2nd)} \rightarrow HSi\text{-}CH_2\text{-Si}_{(2nd)} \quad (19)$$

where $Si_{(2nd)}$ stands for the Si atom in the second layer. The cleavage of Si−Si backbond by CH_2 is responsible for the desorption of some Si atoms as methyl silanes (Figure 8a).

For the Si−$CCCH_3$ surface, silicon radicals are created when the propynyl moieties diffuse and bind to Si atoms of the second layer (Figure 10a) leaving behind a silyl radical. This diffusion step is equivalent to that of the methylated surface (Figure 8). However, silicon backbonds are not broken in this process. Surface SiH groups are created when the silyl radical dehydrogenates the terminal methyl group (Figure 10b). As in the initial stages all of the top Si atoms are bound to propynyl groups (Si−$CCCH_3$), the Si−$CCCH_2$ species thus produced can only bind to the surface by forming pentacoordinted silicon intermediates Si−$CCCH_2$−Si−$CCCH_3$, which sometimes induce the desorption of the •$CCCH_3$ radical leaving on the surface the bicoordinated Si−$CCCH_2$−Si moiety. The •$CCCH_3$ radical thus produced may either desorb directly to the gas phase or it may abstract a H atom from a SiH group or from the terminal methyl groups of the monolayer.

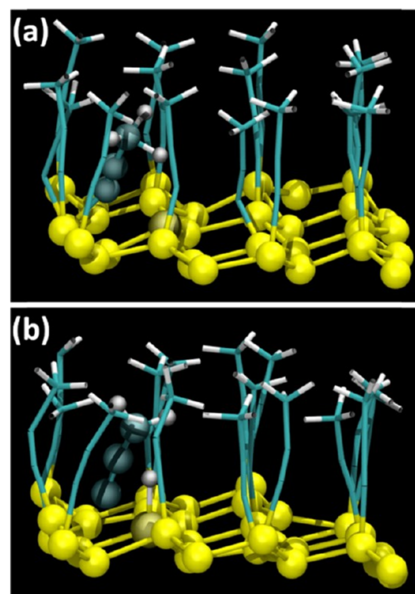

Figure 10. Dehydrogenation of the terminal CH_3 group of propynyl species by a silyl radical. (a) A $CCCH_3$ species originally bound to atop Si atom diffuses to adjacent positions (ball-and-stick model) leaving a silyl radical (dark yellow). (b) SiH group produced after the abstraction of a H atom from the terminal methyl group. Simulation was performed at 1700 K with a $8\sqrt{3} \times 8$ unit cell with 64 Si−$CCCH_3$ groups. Only part of the surface is shown for clarity.

In the case of the 1-propylene monolayer, we observed that silyl radicals never abstracted the H atoms bound to the sp^2 C atoms. The hydrogen abstraction only occurred from the H atoms of the terminal methyl group. However, in this full-coverage monolayer, the Si−$CHCHCH_3$ species are in the trans configuration, which leaves the terminal methyl group away from the surface (Figure 11a). The hydrogen abstraction only takes place after a transition from trans to cis configuration, which leaves the methyl group closer to a silyl radical (Figure 11b). This transition was only observed at the highest temperature. It does not occur at 1500 K and consequently the monolayer is preserved at this temperature as shown in the first panel of Figure 7a. The dehydrogenation of the methyl group produces the bicoordinated Si−$CHCHCH_2$−Si moiety, as shown in Figure 11c. Therefore, the dehydrogenation of the 1-propylene monolayer involves two steps

$$\equiv\text{Si-}CHCHCH_{3(trans)} \rightarrow \equiv \text{Si-}CHCHCH_{3(cis)} \quad (20)$$

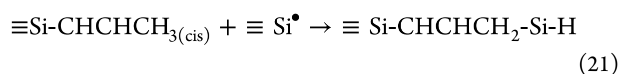

$$\equiv\text{Si-}CHCHCH_{3(cis)} + \equiv Si^{\bullet} \rightarrow \equiv \text{Si-}CHCHCH_2\text{-Si-H} \quad (21)$$

DOI: 10.1021/acsami.7b05444
ACS Appl. Mater. Interfaces 2017, 9, 30969−30981

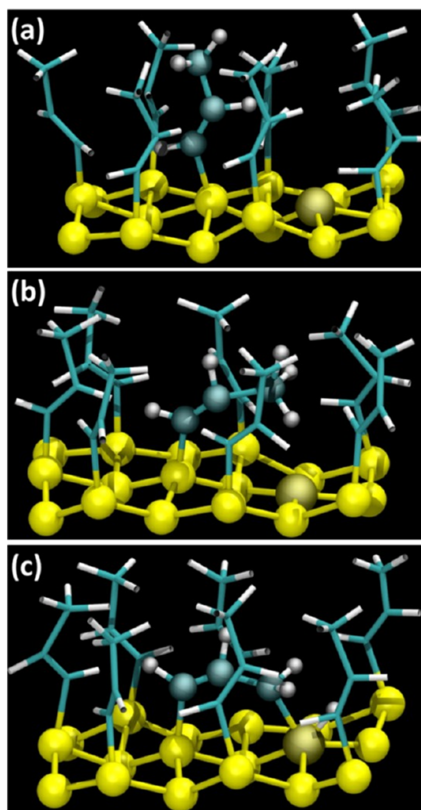

Figure 11. Dehydrogenation of the terminal CH_3 group of a 1-propenyl species by a silyl radical. (a) Silyl radical (dark yellow) adjacent to $CCCH_3$ species (ball-and-stick model) with trans configuration, (b) $CCCH_3$ species with cis configuration, and (c) bicoordinated Si−$CHCHCH_2$−Si.

In the last step, a pentacoordinated Si atom is formed (see Figure 11c). In the initial stages of the simulation, when all top Si atoms are involved in Si−C bonds, the H atom in the pentacoordinated Si atom diffuses to other top Si atoms until it eventually induces a molecular desorption process

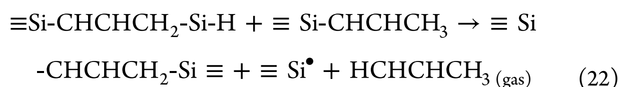

$$\equiv \text{Si-CHCHCH}_2\text{-Si-H} + \equiv \text{Si-CHCHCH}_3 \rightarrow \equiv \text{Si}$$
$$\text{-CHCHCH}_2\text{-Si} \equiv + \equiv \text{Si}^\bullet + \text{HCHCHCH}_{3\,(\text{gas})} \quad (22)$$

Irrespective of the simulation temperature, we observed that silyl radicals only induce the breakage of the C−H bonds of the terminal methyl groups. This correlates with the fact that the C−H bond strength of C atoms with sp^3 hybridization is weaker than for sp^2 C atoms.[50] In summary, the outstanding stability of the 1-propylene monolayer is due to the presence of a rigid backbone with sp^2 C atoms, which (a) make the trans/cis transition very costly and (b) have strong C−H bonds.

Unlike the $-CCCH_3$ monolayer, steric constraints preclude the formation of pentacoordinated intermediates for the $-CHCHCH_3$ monolayer because the $-CHCHCH_3$ moieties are more tightly packed than the $-CCCH_3$ moieties. For the linear $-CCCH_3$, the carbon backbone of adjacent molecules is separated by 3.84 Å, which is the distance between adjacent top Si atoms (Figure S1f). However, the $-CHCHCH_3$ moieties have a nonlinear carbon backbone, which leads to lower distances between the C atoms and H atoms of adjacent molecules (lowest C···C and H···H distances of 3.21 and 2.0 Å, respectively; see Figure S1g). The steric constraints within the $-CHCHCH_3$ layer are also evidenced during the MD simulations. This monolayer has lower fluctuations in the distance between the C atoms of adjacent molecules than the $-CCCH_3$ monolayer.

Our results are in agreement with the trends in stability reported for these layers experimentally.[33] The Si−$CHCHCH_3$ layer was found to show the best passivating behavior as it inhibits silicon oxidation even after more than 2 months of exposure to air,[33] whereas the Si−$CCCH_3$ monolayer oxidized after 25 days and the Si−$CH_2CH_2CH_3$ layer oxidized much faster.[33] The MD simulations show that the compact monolayer structure of Si−$CHCHCH_3$ is the most stable of all layers investigated. Consequently, the diffusion of oxygenated species through this monolayer is expected to be hindered by steric factors. This process has high diffusional energy barriers as we showed in previous work.[39] The fact that the Si−$CCCH_3$ monolayer oxidizes faster than the Si−$CHCHCH_3$ monolayer correlates with the fact that the disordering of the propynyl layer is higher than that of the 1-propenyl layer at the same temperature (Figure 8). For a more disordered monolayer, an easier diffusion of oxidizing species toward silicon atoms is expected. For the same reason, for Si−$CHCHCH_3$ or Si−$CCCH_3$ surfaces with a lower surface coverage (also having SiH groups), we would expect a lower thermal (and also passivating) resistance, as the decrease in surface coverage increases the degrees of freedom, which favor the disordering and finally the decomposition of a layer.

The integrity of organic monolayers is usually evaluated by following the C 1s emission in XPS experiments. We therefore compared the percentage of C atoms remaining on the surface after a simulation time of 800 ps for the different monolayers (Table 1). The stability of the alkyl layers (from C2 to C10)

Table 1. Percentage of C Atoms Remaining on the Surface after a Simulation Time of 800 ps[a]

T (K)	C2	C3	C5	C10	CH_3	$CCCH_3$	$CHCHCH_3$
1500	50	73	64	94	93	92	100
1800	25	40	17	25	100[b]	84	66
2000	12	17	15	8	100[b]	96[b]	85[b]

[a]The reference is the intact monolayer. [b]Formation of SiC.

rapidly decreases with temperature. Only at 1500 K, there is some correlation between the percentage of carbon and the chain length (except for the C3 layer), whereas at the highest temperatures, the C3 layer is the most stable, even more than the C10 layer. This is in agreement with experimental results in which no correlation with the alkyl chain length was observed.[26] As we discussed above, the high stability of the C3 monolayer is due to the presence of stable bicoordinated Si−$CH_2CH_2CH_2$−Si moieties (Figure 6a).

Table 1 shows that the full-coverage monolayers have a higher thermal stability than the n-alkyl monolayers. The methylated layer is a special case because the dehydrogenation of the methyl group leads to carbon species, which insert into the Si−Si bonds to finally yield SiC. Even at simulation times longer than 800 ps, the Si−$CHCHCH_3$ layer remains intact at 1500 K. At the highest temperature, all of the full-coverage monolayers produce different amounts of SiC.

CONCLUSIONS

Using ReaxFF reactive molecular dynamics simulations, we have presented a complete picture of the mechanisms of thermal decomposition of the Si(111) surface grafted with n-

DOI: 10.1021/acsami.7b05444
ACS Appl. Mater. Interfaces 2017, 9, 30969−30981

alkyl chains (50% surface coverage), as well as with the full-coverage methyl, propynyl, and 1-propenyl layers. Our results provide a detailed atomistic interpretation of experimental results by identifying the nature of adsorbed species as well as the desorption products. The structure of the organic chain, the nature of the surface bonding, and the presence of silyl radicals mainly dictate the thermal stability of the grafted surfaces.

Si radicals play a key role in the dehydrogenation processes that lead to the decomposition of the monolayers. Initially, they are produced by the breakage of Si−C bonds, which leads to direct desorption of the corresponding organic radical to the gas phase. The number of silyl radicals remains approximately constant during the simulations with a concentration of less than 10% of the top Si atoms.

The dehydrogenation pathways depend on the nature of the organic molecule. Silyl radicals may abstract H atoms from any methylene group of n-alkyl chains due to their flexibility. However, the most common pathway is dehydrogenation from the β carbon, which leads to desorption of the corresponding 1-alkene. This process involves two surface Si atoms rather than one, as proposed in the literature.[23−25] Dehydrogenation of other methylene groups produces bicoordinated molecules on the surface, cleavage of C−C bonds, or formation of terminal vinyl groups. This suggests that controlled thermal treatments of long-chain alkyl layers could be used to introduce reactive functionalities, such as the vinyl group. The alkylated surfaces finally end mostly hydrogenated with the silicon surface keeping its 111 periodicity.

Silyl radicals are also involved in the dehydrogenation of the full-coverage methyl, propynyl, and 1-propenyl monolayers, yielding stable bicoordinated Si−CH_2−Si, Si−CCCH_2−Si, and Si−CHCHCH_2−Si moieties. Consequently, the desorption of carbon-containing gas-phase products is considerably lower than for the n-alkyl monolayers. The rigid carbon backbone of the 1-propenyl layer keeps the terminal methyl group away from adjacent silyl radicals, which considerably delays the dehydrogenation of this monolayer.

In summary, the thermal stability of an organic layer bound to silicon via Si−C bonds depends on the rate of dehydrogenation reactions. Any process retarding the dehydrogenation can improve the thermal stability of the layer. Molecules having a rigid backbone close to the Si surface are expected to have a higher thermal stability as is the case for the 1-propenyl monolayer. On the contrary, the flexibility of the n-alkyl chains favors the dehydrogenation and rapid decomposition of these monolayers.

The ability of the Si/C/H ReaxFF potential to describe the rich chemistry of functionalized silicon surfaces opens new avenues to investigate functionalized silicon nanostructures, such as quantum dots. Future extensions including the O atom will allow reactive molecular dynamic investigations, involving the environment (H_2O and O_2), reactive terminal groups (−COOH, −OH, etc.), and silicon grafting via the Si−OR bond.

■ ASSOCIATED CONTENT

Supporting Information

The Supporting Information is available free of charge on the ACS Publications website at DOI: 10.1021/acsami.7b05444.

Initial structures of molecules on the Si(111) surface and snapshots of molecular dynamics simulations (PDF)

■ AUTHOR INFORMATION

Corresponding Author

*E-mail: martin@fcq.unc.edu.ar.

ORCID

Weiwei Zhang: 0000-0002-5255-7340

Eduardo M. Patrito: 0000-0002-5817-966X

Notes

The authors declare no competing financial interest.

■ ACKNOWLEDGMENTS

E.M.P. and F.A.S. acknowledge Conicet (PIP 5903), Secyt-UNC, and Foncyt (PICT-2014-2199) for financial support. A.C.T.v.D. and W.Z. acknowledge funding from NSF grant #1462980. This work used computational resources from CCAD—Universidad Nacional de Córdoba (http://ccad.unc.edu.ar/), which is part of SNCAD—MinCyT, República Argentina.

■ REFERENCES

(1) Linford, M. R.; Chidsey, C. E. D. Alkyl Monolayers Covalently Bonded to Silicon Surfaces. *J. Am. Chem. Soc.* **1993**, *115*, 12631.

(2) Ciampi, S.; Harper, J. B.; Gooding, J. J. Wet Chemical Routes to the Assembly of Organic Monolayers on Silicon Surfaces via the Formation of Si−C Bonds: Surface Preparation, Passivation and Functionalization. *Chem. Soc. Rev.* **2010**, *39*, 2158−2183.

(3) Buriak, J. M. Illuminating Silicon Surface Hydrosilylation: An Unexpected Plurality of Mechanisms. *Chem. Mater.* **2014**, *26*, 763−772.

(4) DeBenedetti, W. J. I.; Chabal, Y. J. Functionalization of Oxide-free Silicon Surfaces. *J. Vac. Sci. Technol., A* **2013**, *31*, No. 050826.

(5) Fabre, B. Functionalization of Oxide-Free Silicon Surfaces with Redox-Active Assemblies. *Chem. Rev.* **2016**, *116*, 4808−4849.

(6) Wong, K. T.; Lewis, N. S. What a Difference a Bond Makes: The Structural, Chemical, and Physical Properties of Methyl-Terminated Si(111) Surfaces. *Acc. Chem. Res.* **2014**, *47*, 3037−3044.

(7) Scheres, L.; Giesbers, M.; Zuilhof, H. Organic Monolayers onto Oxide-Free Silicon with Improved Surface Coverage: Alkynes versus Alkenes. *Langmuir* **2010**, *26*, 4790−4795.

(8) Scheres, L.; Giesbers, M.; Zuilhof, H. Self-Assembly of Organic Monolayers onto Hydrogen-Terminated Silicon: 1-Alkynes Are Better Than 1-Alkenes. *Langmuir* **2010**, *26*, 10924−10929.

(9) Cheng, X.; Lowe, S. B.; Reece, P. J.; Gooding, J. J. Colloidal Silicon Quantum Dots: From Preparation to the Modification of Self-Assembled Monolayers (SAMs) for Bio-Applications. *Chem. Soc. Rev.* **2014**, *43*, 2680−2700.

(10) Paul, A.; Jana, A.; Karthik, S.; Bera, M.; Zhao, Y.; Singh, N. D. P. Photoresponsive Real Time Monitoring Silicon Quantum Dots for Regulated Delivery of Anticancer Drugs. *J. Mater. Chem. B* **2016**, *4*, 521−528.

(11) Kang, O. S.; Bruce, J. P.; Herbert, D. E.; Freund, M. S. Covalent Attachment of Ferrocene to Silicon Microwire Arrays. *ACS Appl. Mater. Interfaces* **2015**, *7*, 26959−26967.

(12) Ciampi, S.; Choudhury, M. H.; Ahmad, S. A. B. A.; Darwish, N.; Brun, A. L.; Gooding, J. J. The Impact of Surface Coverage on the Kinetics of Electron Transfer through Redox Monolayers on a Silicon Electrode Surface. *Electrochim. Acta* **2015**, *186*, 216−222.

(13) Dasog, M.; De los Reyes, G. B.; Titova, L. V.; Hegmann, F. A.; Veinot, J. G. C. Size vs Surface: Tuning the Photoluminescence of Freestanding Silicon Nanocrystals Across the Visible Spectrum via Surface Groups. *ACS Nano* **2014**, *8*, 9636−9648.

(14) Dasog, M.; Kehrle, J.; Rieger, B.; Veinot, J. G. C. Silicon Nanocrystals and Silicon-Polymer Hybrids: Synthesis, Surface Engineering, and Applications. *Angew. Chem., Int. Ed.* **2016**, *55*, 2322−2339.

(15) Fermi, A.; Locritani, M.; Di Carlo, G.; Pizzotti, M.; Caramori, S.; Yu, Y.; Korgel, B. A.; Bergamini, G.; Ceroni, P. Light-Harvesting

Antennae Based on Photoactive Silicon Nanocrystals Functionalized with Porphyrin Chromophores. *Faraday Discuss.* **2015**, *185*, 481−495.
(16) Peng, F.; Su, Y.; Zhong, Y.; Fan, C.; Lee, S.-T.; He, Y. Silicon Nanomaterials Platform for Bioimaging, Biosensing, and Cancer Therapy. *Acc. Chem. Res.* **2014**, *47*, 612−623.
(17) Kanyong, P.; Sun, G.; Rösicke, F.; Syritski, V.; Panne, U.; Hinrichs, K.; Rappich, J. Maleimide Functionalized Silicon Surfaces for Biosensing Investigated by in-Situ IRSE and EQCM. *Electrochem. Commun.* **2015**, *51*, 103−107.
(18) Peng, W.; Rupich, S. M.; Shafiq, N.; Gartstein, Y. N.; Malko, A. V.; Chabal, Y. J. Silicon Surface Modification and Characterization for Emergent Photovoltaic Applications Based on Energy Transfer. *Chem. Rev.* **2015**, *115*, 12764−12796.
(19) Markov, I. L. Limits on Fundamental Limits to Computation. *Nature* **2014**, *512*, 147−154.
(20) Dusciac, D.; Brize, V.; Chazalviel, J.-N.; Lai, Y.-F.; Roussel, H.; Blonkowski, S.; Schafranek, R.; Klein, A.; Henry de Villeneuve, C.; Allongue, P. Chemical Grafting on Si for Interfacial SiO_2 Growth Inhibition During Chemical Vapor Deposition of HfO_2. *Chem. Mater.* **2012**, *24*, 3135−314.
(21) O'Leary, L. E.; Strandwitz, N. C.; Roske, C. W.; Pyo, S.; Brunschwig, B. S.; Lewis, N. S. Use of Mixed CH_3−/HC(O)-CH_2CH_2−Si(111) Functionality to Control Interfacial Chemical and Electronic Properties During the Atomic-Layer Deposition of Ultrathin Oxides on Si(111). *J. Phys. Chem. Lett.* **2015**, *6*, 722−726.
(22) Yang, F.; Allongue, P.; Ozanam, F.; Chazalviel, J.-N. Thermal Stability of Organic Monolayers Covalently Grafted on Silicon Surfaces. In *Reactions and Mechanisms in Thermal Analysis of Advanced Materials*; Tiwari, A., Raj, B., Eds.; John Wiley & Sons: Massachusetts, 2015; pp 3−37. See also references therein.
(23) Sung, M. M.; Kluth, G. J.; Yauw, O. W.; Maboudian, R. Thermal Behavior of Alkyl Monolayers on Silicon Surfaces. *Langmuir* **1997**, *13*, 6164−6168.
(24) Faucheux, A.; Gouget-Laemmel, A. C.; Allongue, P.; de Villeneuve, C. H.; Ozanam, F.; Chazalviel, J. N. Mechanisms of Thermal Decomposition of Organic Monolayers Grafted on (111) Silicon. *Langmuir* **2007**, *23*, 1326−1332.
(25) Jaeckel, B.; Hunger, R.; Webb, L. J.; Jaegermann, W.; Lewis, N. S. High-Resolution Synchrotron Photoemission Studies of the Electronic Structure and Thermal Stability of CH_3- and C_2H_5-Functionalized Si(111) Surfaces. *J. Phys. Chem. C* **2007**, *111*, 18204−18213.
(26) Yamada, R.; Ara, M.; Tada, H. Temperature Dependence of the Structure of Alkyl Monolayers on Si(111) Surface via Si−C Bond by ATR-FT-IR Spectroscopy. *Chem. Lett.* **2004**, *33*, 492−493.
(27) Faucheux, A.; Yang, F.; Allongue, P.; Henry de Villeneuve, C.; Ozanam, F.; Chazalviel, J.-N. Thermal Decomposition of Alkyl Monolayers Covalently Grafted on (111) Silicon. *Appl. Phys. Lett.* **2006**, *88*, No. 193123.
(28) Hunger, R.; Fritsche, R.; Jaeckel, B.; Jaegermann, W.; Webb, L. J.; Lewis, N. S. Chemical and Electronic Characterization of Methyl-Terminated Si(111) Surfaces by High-Resolution Synchrotron Photoelectron Spectroscopy. *Phys. Rev. B* **2005**, *72*, No. 045317.
(29) Yu, H.; Webb, L. J.; Ries, R. S.; Solares, S. D.; Goddard, W. A.; Heath, J. R.; Lewis, N. S. Low-temperature STM Images of Methyl-Terminated Si(111) Surfaces. *J. Phys. Chem. B* **2005**, *109*, 671−674.
(30) Yang, F.; Hunger, R.; Roodenko, K.; Hinrichs, K.; Rademann, K.; Rappich, J. Vibrational and Electronic Characterization of Ethynyl Derivatives Grafted onto Hydrogenated Si(111) Surfaces. *Langmuir* **2009**, *25*, 9313−9318.
(31) Salingue, N.; Hess, P. Preparation, IR spectroscopy, and Time-of-Flight Mass Spectrometry of Halogenated and Methylated Si(111). *Appl. Phys. A* **2011**, *104*, 987−991.
(32) Hurley, P. T.; Nemanick, E. J.; Brunschwig, B. S.; Lewis, N. S. Covalent Attachment of Acetylene and Methylacetylene Functionality to Si(111) Surfaces: Scaffolds for Organic Surface Functionalization While Retaining Si−C Passivation of Si(111) Surface Sites. *J. Am. Chem. Soc.* **2006**, *128*, 9990−9991.
(33) Puniredd, S. R.; Assad, O.; Haick, H. Highly Stable Organic Monolayers for Reacting Silicon with Further Functionalities: The Effect of the C−C Bond Nearest the Silicon Surface. *J. Am. Chem. Soc.* **2008**, *130*, 13727−13734.
(34) Plymale, N. T.; Kim, Y.-G.; Soriaga, M. P.; Brunschwig, B. S.; Lewis, N. S. Synthesis, Characterization, and Reactivity of Ethynyl- and Propynyl-Terminated Si(111) Surfaces. *J. Phys. Chem. C* **2015**, *119*, 19847−19862.
(35) Takeuchi, N.; Kanai, Y.; Selloni, A. Surface Reaction of Alkynes and Alkenes with H-Si(111): A Density Functional Theory Study. *J. Am. Chem. Soc.* **2004**, *126*, 15890−15896.
(36) Kanai, Y.; Selloni, A. Competing Mechanisms in the Optically Activated Functionalization of the Hydrogen-Terminated Si(111) Surface. *J. Am. Chem. Soc.* **2006**, *128*, 3892−3893.
(37) Juarez, M. F.; Soria, F. A.; Patrito, E. M.; Paredes-Olivera, P. Influence of Subsurface Oxidation on the Structure, Stability, and Reactivity of Grafted Si(111) Surfaces. *J. Phys. Chem. C* **2008**, *112*, 14867−14877.
(38) Soria, F. A.; Patrito, E. M.; Paredes-Olivera, P. Oxidation of Hydrogenated Si(111) by a Radical Propagation Mechanism. *J. Phys. Chem. C* **2012**, *116*, 24607−24615.
(39) Soria, F. A.; Paredes-Olivera, P.; Patrito, E. M. Chemical Stability toward O_2 and H_2O of Si(111) Grafted with $-CH_3$, $-CH_2CH_2CH_3$, $-CHCHCH_3$, and $-CCCH_3$. *J. Phys. Chem. C* **2015**, *119*, 284−295.
(40) Soria, F. A.; Patrito, E. M.; Paredes-Olivera, P. On the Mechanism of Silicon Activation by Halogen Atoms. *Langmuir* **2011**, *27*, 2613−2624.
(41) Soria, F. A.; Patrito, E. M.; Paredes-Olivera, P. Tailoring the Surface Reactivity of Silicon Surfaces by Partial Halogenation. *J. Phys. Chem. C* **2013**, *117*, 18021−18030.
(42) Senftle, T. P.; Hong, S.; Islam, M. M.; Kylasa, S. B.; Zheng, Y.; Shin, Y. K.; Junkermeier, C.; Engel-Herbert, R.; Janik, M. J.; Aktulga, H. M.; Verstraelen, T.; Grama, A.; van Duin, A. C. T. The ReaxFF Reactive Force-Field: Development, Applications and Future Directions. *npj Comput. Mater.* **2016**, *2*, No. 15011.
(43) van Duin, A. C. T.; Dasgupta, S.; Lorant, F.; Goddard, W. A. ReaxFF: A Reactive Force Field for Hydrocarbons. *J. Phys. Chem. A* **2001**, *105*, 9396−9409.
(44) Chenoweth, K.; van Duin, A. C. T.; Goddard, W. A. ReaxFF Reactive Force Field for Molecular Dynamics Simulations of Hydrocarbon Oxidation. *J. Phys. Chem. A* **2008**, *112*, 1040−1053.
(45) Soria, F. A.; Zhang, W.; van Duin, A. C. T.; Patrito, E. M. A Si/C/H Reactive Potential for Silicon Surfaces Grafted with Organic Molecules, in preparation.
(46) ADF. *Molecular Modeling Suite, Scientific Computing and Modeling*; Vrije Universiteit: Amsterdam, The Netherlands, 2016. http://www.scm.com.
(47) Plimpton, S. Fast Parallel Algorithms for Short-Range Molecular Dynamics. *J. Comput. Phys.* **1995**, *117*, 1−19.
(48) Sattar, Md. A.; Hien, K. T. T.; Miyauchi, Y.; Mizutani, G.; Rutt, H. N. Hydrogen Desorption Kinetics from H−Si(111) Surfaces Studied by Optical Sum Frequency Generation and Second Harmonic Generation. *Surf. Interface Anal.* **2016**, *48*, 1235−1239.
(49) Guo, H.; Farjamnia, A.; Jackson, B. Effects of Lattice Motion on Dissociative Chemisorption: Toward a Rigorous Comparison of Theory with Molecular Beam Experiments. *J. Phys. Chem. Lett.* **2016**, *7*, 4576−4584.
(50) Blanksby, S. J.; Ellison, G. B. Dissociation Energies of Organic Molecules. *Acc. Chem. Res.* **2003**, *36*, 255−263.

DOI: 10.1021/acsami.7b05444
ACS Appl. Mater. Interfaces 2017, 9, 30969−30981